*Journal of Sound and Vibration* (1998) **217**(2), 297–320
*Article No*. sv981761

# FREE VIBRATION OF THIN, ISOTROPIC, OPEN, CONICAL PANELS

N. S. Bardell, J. M. Dunsdon and R. S. Langley

*Department of Aeronautics and Astronautics*, *University of Southampton*, *Highfield*, *Southampton SO*17 1*BJ*, *England*

(*Received* 18 *December* 1997, *and in final form* 20 *May* 1998)

This paper describes a general analysis of the vibration characteristics of thin, open, conical isotropic panels using the *h-p* version of the finite element method in conjunction with Love's thin shell equations. The convergence properties of this element have been established for particular geometries, thereby endorsing its suitability for use in further parameter studies. Natural frequencies and modes have been obtained for two completely free panels using (i) the *h-p* methodology reported here, (ii) a commercially available finite element package, and (iii) experimental work. Excellent agreement has been found between all three approaches. Some further comparisons with the work of other investigators have also been performed, and generally good agreement has been found. Finally, a brief parameter study has been presented for clamped and simply supported open conical panels with an included angle of $\pi/3$, whose semi-vertex angle has been varied continuously between 0 and $\pi/2$. It is noted that the methodology advanced here for a generic conical panel can also be used to analyse the dynamic behaviour of *closed* conical frusta, open or closed cylindrical shells, and flat annular sectorial plates.



## 1. INTRODUCTION

Open conical panels, consisting of a segment of a complete conical shell, are commonly found in a variety of engineering applications, sometimes as stand-alone items, but more often than not as a component of a larger, built-up structure. A good example of this latter type of construction is the tapering tail section of a civil aircraft's fuselage. In service, such panels are often subjected to a variety of different fluctuating loads, and it is essential that their dynamic integrity can be assured from the design stage onwards. To this end, it is important that reliable predictive techniques are available; hence it may come as something of a surprise to realize that as recently as 1981, a comprehensive survey conducted by Chang [1] echoed the conclusions drawn a decade earlier by Leissa [2], that "strangely, no references have been found which deal explicitly with the free

0022–460X/98/420297 + 24 $30.00/0 

vibrations of such [open conical] shells''. The most likely reason for this lacuna concerns the analytical difficulties involved; for a completely closed, right circular cone or frustum, the two-dimensional nature of the assumed displacement field can be reduced to a quasi one-dimensional problem through Fourier decomposition of the circumferential wavemotion—for an *open* conical panel, no such simplification exists, and resort must be made to a full two-dimensional solution scheme.

Love [3] is generally credited with being the first investigator to provide a general set of equations expressing both the extension, and the changes in curvature, of an arbitrarily curved thin shell subject to small displacements. During the 1930s, Love's work found application to the vibration of completely closed, right circular cones and frusta in the context of loudspeaker design [4–6]. However, it was not until the 1950s, when the space-age began in earnest, that further interest was shown in such shells on account of their widespread utilization in the design of space vehicles. Comprehensive literature reviews of this era have been compiled by Hu [7], Tang [8], Weingarten [9], and Leissa [2], and more recently by Liew *et al*. [10].

Returning to the privative topic of *open* conical panels, only *three*† directly relevant publications could be found at the time of writing. A brief review of these papers is included here to assess their contribution to the literature, and to help position the current work.

The first free vibration analysis *per se* was reported by Srinivasan and Krishnan [13], who sought the natural frequencies and modes of clamped isotropic conical panels using Donnell's shell theory and an integral equation technique. Unfortunately, the convergence study presented by these authors to justify the number of terms used in their subsequent parameter study is of doubtful validity, and hence some caution must be exercised if these latter results are to be used as a benchmark.

Cheung *et al*. [14] developed a spline finite strip method which could be applied to a variety of singly curved shells. They used the results from one of Srinivasan and Krishnan's examples to validate the applicability of their general spline technique to conical panels (among others), and demonstrated significantly better convergence than the previous authors. It is also worth noting that Cheung *et al*. comment on the fact that ''readers can also note that the results of Srinivasan and Krishnan do not seem to have yet converged and in any case the convergence is not monotonic''.

More recently, Lim and Liew [15] have produced a simplified vibration analysis of a conical panel by modelling it as a *shallow* shell with a *trapezoidal* projected planform. This simplification results in a far more tractable problem than a conventional cone analysis, and enabled them to produce verifiable results for panels whose curved ends subtended angles up to $30^\circ$. The ubiquitous *pb*-2 shape functions were used to represent the assumed displacement field of the panel (for specific edge conditions), and a Rayleigh–Ritz method furnished the natural

†Although the seminal works of Rossettos and Parisse [11], and Teichmann [12], are not of immediate relevance to the title problem, both items deserve a mention because they are the earliest pieces of work that specifically address the dynamic response of open conical panels.

frequencies by minimizing the energy functional. Their work showed good agreement with that of Cheung *et al*. [14], and provided the first known set of parameter studies and modes for a limited class of conical panels.

Subsequent work by Liew and his co-workers has addressed some interesting issues related to shallow conical shells, such as the effects of initial twist and thickness variation [16], through-the-thickness shear flexibility [17], and layered composite construction [18]. However, all this work is based on the same premise of a *shallow* shell with a *trapezoidal* planform that was developed in [15]; no matter which of these special cases is chosen therefore, nothing fundamentally new is contributed to the problem under investigation here.

Clearly, there is scope for further work in this subject area, especially with regard to the following points: (i) the effect on natural frequencies of different combinations of edge boundary conditions, in conjunction with variations of the governing geometric parameters, (ii) the development, and validation, of alternative analysis techniques for non-shallow conical panels, and (iii) some experimental verification of the results forthcoming from (i) and (ii).

The purpose of this paper is to provide partial fulfilment of all three of these categories by developing a solution strategy based on the *h-p* version of the finite element method [19, 20], presenting a selection of frequency and mode results from the analysis, and providing some initial experimental results for validation purposes. The novelty of the solution scheme is further enhanced by the use of the highly versatile set of trigonometric *p*-functions first proposed by Beslin and Nicolas [21].

## 2. METHOD OF ANALYSIS

An *h-p* version of the finite element method is developed here in order to afford the user a robust, flexible, and economic analysis tool that can accommodate geometric irregularities such as cut-outs. The *h-p* methodology adopted here is similar to that presented elsewhere by the authors [22], so only the essential details are given here.

Consider the thin conical shell element shown in Figure 1, whose middle surface is defined by the semi-vertex angle $\alpha$, the radius of curvature at any point $R(x) = R_0 + x \sin \alpha$ (where $R_0$ is the radius of curvature of the small end), the slant length $a$ and the total included angle $\phi$. The cone is assumed to be of uniform thickness $h$ (with $h/R(x)$ assumed to be small for all $x$). The components of displacement of a point on the middle surface are $u$, $v$ and $w$ in the $x$, $\theta$, and $z$ directions, respectively.

The state of strain at any point $x$, $\theta$ within the shell, distance $z$ from the middle surface, is equal to the sum of the middle surface (membrane or extensional) strains and the (flexural or inextensional) strains due to the changes of curvature. Denoting the middle surface extensional strains in the lengthwise and circumferential directions by $\varepsilon^0_{xx}$, $\varepsilon^0_{\theta\theta}$, the middle surface changes in curvature in the lengthwise and circumferential directions by $\kappa^0_{xx}$, $\kappa^0_{\theta\theta}$, and the middle surface in-plane shear strain and change in twist by $\gamma^0_{x\theta}$, $\kappa^0_{x\theta}$ respectively, then the state of

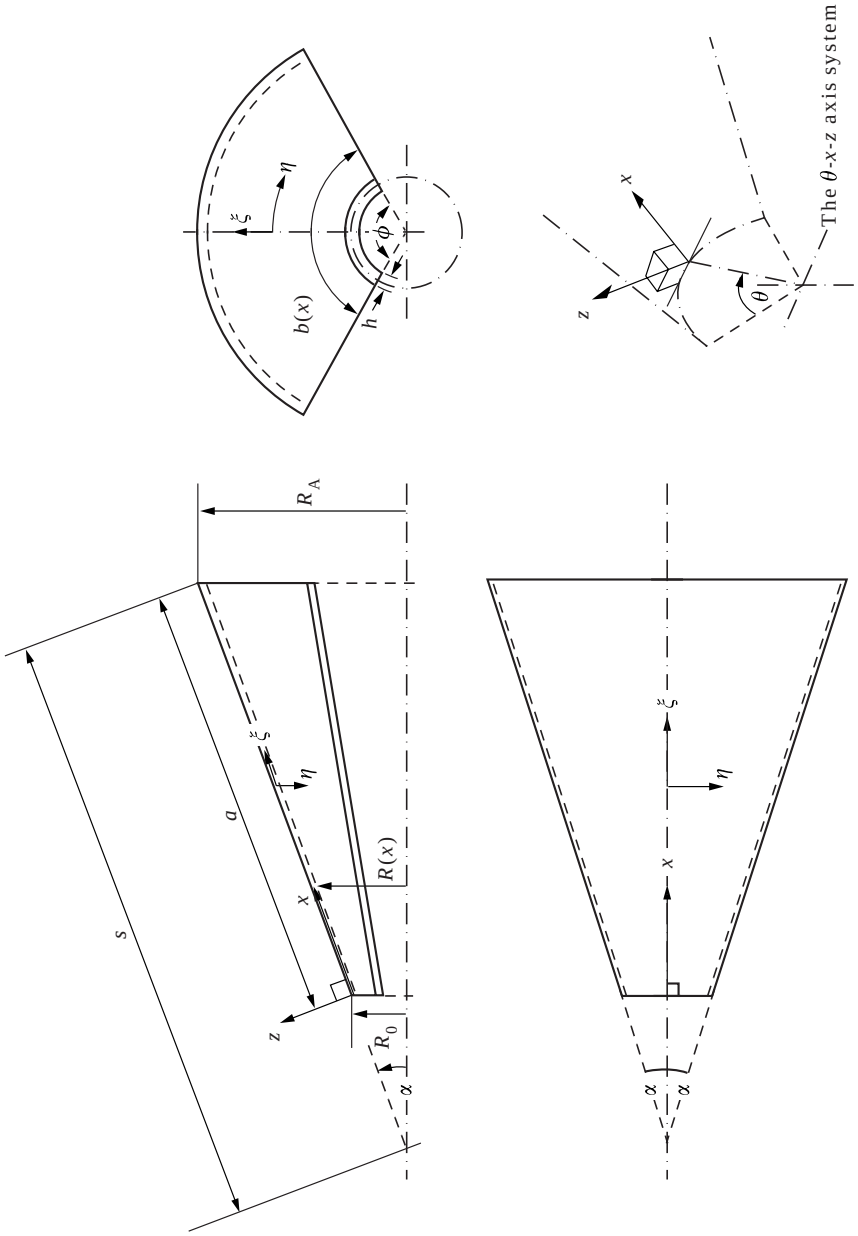


Figure 1. The geometry defining a thin conical shell.

strain at any point $x$, $\theta$, $z$ within the shell can be written:

$$\varepsilon_{xx} = \varepsilon^0_{xx} + z\kappa^0_{xx}$$

$$\varepsilon_{\theta\theta} = \varepsilon^0_{\theta\theta} + z\kappa^0_{\theta\theta} \tag{1}$$

$$\gamma_{x\theta} = \gamma^0_{x\theta} + 2z\kappa^0_{x\theta}$$

where, for a cone [3, 23],

$$\varepsilon^0_{xx} = \frac{\partial u}{\partial x}$$

$$\varepsilon^0_{\theta\theta} = \frac{1}{R(x)}\frac{\partial v}{\partial \theta} + u\frac{\sin\alpha}{R(x)} + w\frac{\cos\alpha}{R(x)}$$

$$\gamma^0_{x\theta} = \frac{\partial v}{\partial x} + \frac{1}{R(x)}\frac{\partial u}{\partial \theta} - v\frac{\sin\alpha}{R(x)} \tag{2}$$

$$\kappa^0_{xx} = -\frac{\partial^2 w}{\partial x^2}$$

$$\kappa^0_{\theta\theta} = -\frac{1}{R(x)^2}\frac{\partial^2 w}{\partial \theta^2} + \frac{\cos\alpha}{R(x)^2}\frac{\partial v}{\partial \theta} - \frac{\sin\alpha}{R(x)}\frac{\partial w}{\partial x}$$

$$\kappa^0_{x\theta} = \frac{\sin\alpha}{R(x)^2}\frac{\partial w}{\partial \theta} - \frac{1}{R(x)}\frac{\partial^2 w}{\partial x\,\partial \theta} + \frac{\cos\alpha}{R(x)}\frac{\partial v}{\partial x} - v\frac{\cos\alpha\sin\alpha}{R(x)^2}$$

and $u$, $v$, and $w$ are the mid-plane ($z = 0$) displacements. The full kinematic relationships between the displacements at a general point $x$, $\theta$, $z$, and the mid-plane displacements $u$, $v$, $w$ are given in [23].

By substituting equation (2) into equations (1), and introducing the non-dimensional element-local co-ordinates $\xi$, $\eta$ which are related to the element Cartesian co-ordinates through $\xi = (2x/a) - 1$ and $\eta = (2\theta/\phi) - 1$ (see Figure 1), the strain–displacement relationship can be rendered in the following matrix form:

$$\begin{bmatrix} \varepsilon_{xx} \\ \varepsilon_{\theta\theta} \\ \gamma_{x\theta} \end{bmatrix} = \begin{bmatrix} \dfrac{2}{a}\dfrac{\partial}{\partial\xi} & 0 & -z\dfrac{4}{a^2}\dfrac{\partial^2}{\partial\xi^2} \\ \phi\dfrac{\sin\alpha}{b(x)} & \dfrac{2}{b(x)}\left(1+z\phi\dfrac{\cos\alpha}{b(x)}\right)\dfrac{\partial}{\partial\eta} & \phi\dfrac{\cos\alpha}{b(x)} - z\dfrac{4}{b(x)^2}\dfrac{\partial^2}{\partial\eta^2} - z\phi\dfrac{2\sin\alpha}{ab(x)}\dfrac{\partial}{\partial\xi} \\ \dfrac{2}{b(x)}\dfrac{\partial}{\partial\eta} & \dfrac{2}{a}\dfrac{\partial}{\partial\xi} - \phi\dfrac{\sin\alpha}{b(x)} - z\phi^2\dfrac{2\cos\alpha\sin\alpha}{b(x)^2} + z\phi\dfrac{4\cos\alpha}{ab(x)}\dfrac{\partial}{\partial\xi} & -z\dfrac{8}{ab(x)}\dfrac{\partial^2}{\partial\xi\,\partial\eta} + z\phi\dfrac{4\sin\alpha}{b(x)^2}\dfrac{\partial}{\partial\eta} \end{bmatrix} \begin{bmatrix} u(\xi,\eta) \\ v(\xi,\eta) \\ w(\xi,\eta) \end{bmatrix}, \quad (3)$$

i.e. $\boldsymbol{\varepsilon} = \boldsymbol{\Delta\delta}$

Note that every occurrence of $R(x)$ in equation (3) has been replaced by $b(x)/\phi$ so that there is only one $x$-dependent term in the coefficient of each differential operator. (Note also that the circumferential arc length of the cone, $b(x) \equiv b(\xi)$.)

For an isotropic material, the well-known constitutive relationship is given by

$$\begin{bmatrix} \sigma_{xx} \\ \sigma_{\theta\theta} \\ \tau_{x\theta} \end{bmatrix} = \frac{E}{(1-\nu^2)} \begin{bmatrix} 1 & \nu & 0 \\ \nu & 1 & 0 \\ 0 & 0 & \dfrac{(1-\nu)}{2} \end{bmatrix} \begin{bmatrix} \varepsilon_{xx} \\ \varepsilon_{\theta\theta} \\ \gamma_{x\theta} \end{bmatrix}$$

$$\text{i.e.,} \quad \boldsymbol{\sigma} = \mathbf{D}\boldsymbol{\varepsilon}. \tag{4}$$

For the type of problem under consideration, it is advantageous to use the *same* set of assumed displacement functions to represent the motions in all three co-ordinate directions. To this end, as ascending hierarchy of special trigonometric functions [21], used in conjunction with Hermite cubics, will furnish a robust complete set of admissible displacement functions, $f(\xi$ or $\eta)$. (This set is

TABLE 1

*The first ten assumed displacement functions*

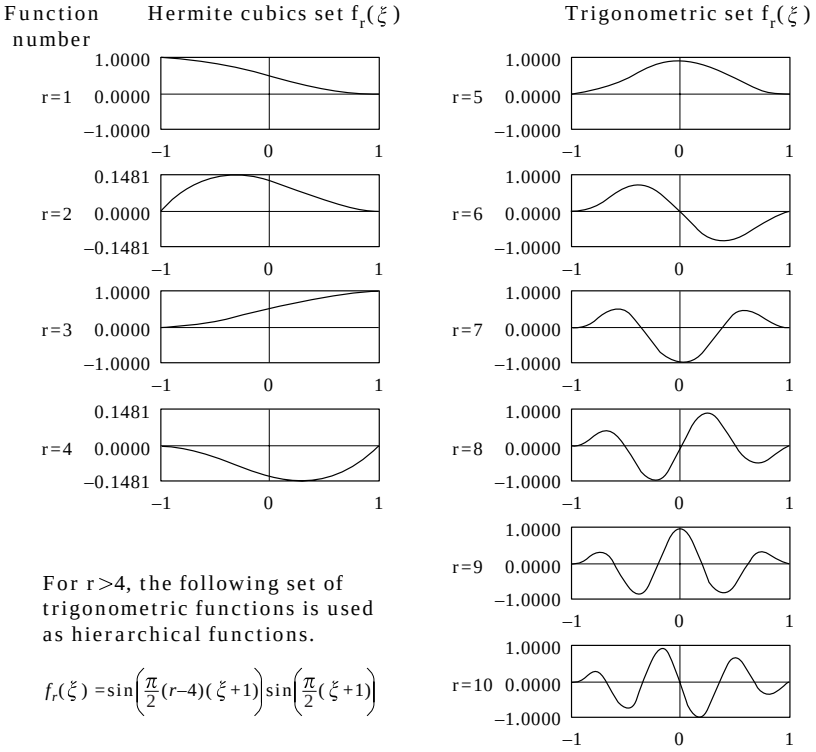

summarized in Table 1.) Hence the in-plane displacement fields $u$ and $v$, and the out-of-plane displacement field $w$, may approximately be represented as follows:

$$u(\xi, \eta) = \sum_{r=1}^{p_{ux}} \sum_{s=1}^{p_{u\theta}} X_{r,s} f_r(\xi) f_s(\eta)$$

$$v(\xi, \eta) = \sum_{r=1}^{p_{vx}} \sum_{s=1}^{p_{v\theta}} Y_{r,s} f_r(\xi) f_s(\eta)$$

$$w(\xi, \eta) = \sum_{r=1}^{p_{wx}} \sum_{s=1}^{p_{w\theta}} Z_{r,s} f_r(\xi) f_s(\eta). \tag{5}$$

The nodal displacements/rotations, and the amplitudes of the hierarchical functions along the edges and in the interior of the panel element, $X_{r,s}$, $Y_{r,s}$ and $Z_{r,s}$ constitute the generalized co-ordinates of the problem. (Note: the in-plane degrees of freedom only require compatibility of the $u$- and $v$-displacements to effect $C_0$ continuity; there is no requirement to match the first derivatives of these in-plane functions.) Each summation which appears in equation (5) is taken over [any number of] $p$ assumed modes; the first subscript on $p$ denotes the type of displacement field and the second denotes whether it is in the $x$- or $\theta$-direction. Equation (5) can be written more succinctly in matrix notation as

$$\boldsymbol{\delta} = \mathbf{N}\mathbf{q} \tag{6}$$

where $\boldsymbol{\delta} = \{u(\xi, \eta), v(\xi, \eta), w(\xi, \eta)\}^{\mathrm{T}}$, $\mathbf{q} = \{X_{r,s}, Y_{r,s}, Z_{r,s}\}^{\mathrm{T}}$ and $\mathbf{N}$ is a rectangular matrix containing the shape functions. Hence, the strain energy of the conical panel element, which is given by

$$U = \frac{1}{2} \int_{-1}^{1} \int_{-1}^{1} \int_{-h/2}^{h/2} \boldsymbol{\varepsilon}^{\mathrm{T}} \boldsymbol{\sigma} \frac{ab(\xi)}{4} \, \mathrm{d}z \, \mathrm{d}\eta \, \mathrm{d}\xi, \tag{7}$$

can be constructed from equations (3), (4) and (6). Thus

$$U = \frac{1}{2} \mathbf{q}^{\mathrm{T}} \left[ \frac{a}{4} \int_{-1}^{1} \int_{-1}^{1} \int_{-h/2}^{h/2} [\boldsymbol{\Delta}\mathbf{N}]^{\mathrm{T}} \mathbf{D} [\boldsymbol{\Delta}\mathbf{N}] b(\xi) \, \mathrm{d}z \, \mathrm{d}\eta \, \mathrm{d}\xi \right] \mathbf{q}. \tag{8}$$

The term in the square brackets can be identified as the element stiffness matrix $\mathbf{K}^{\mathrm{E}}$ of the conical panel.

Similarly, the kinetic energy of the thin conical panel element is given by

$$T = \frac{1}{2} \rho \int_{-1}^{1} \int_{-1}^{1} \int_{-h/2}^{h/2} \dot{\boldsymbol{\delta}}^{\mathrm{T}} \dot{\boldsymbol{\delta}} \frac{ab(\xi)}{4} \, \mathrm{d}z \, \mathrm{d}\eta \, \mathrm{d}\xi. \tag{9}$$

Substituting equation (6) into equation (9) yields

$$T = \frac{1}{2} \dot{\mathbf{q}}^{\mathrm{T}} \left[ \rho \frac{a}{4} \int_{-1}^{1} \int_{-1}^{1} \int_{-h/2}^{h/2} \mathbf{N}^{\mathrm{T}} \mathbf{N} b(\xi) \, \mathrm{d}z \, \mathrm{d}\eta \, \mathrm{d}\xi \right] \dot{\mathbf{q}}. \tag{10}$$

Evidently, the term in the square brackets is the element mass matrix $\mathbf{M}^{\mathrm{E}}$ of the conical panel.

Initial attempts to carry out the matrix multiplication and integration required to evaluate $\mathbf{K}^{E}$ and $\mathbf{M}^{E}$ symbolically, in the manner described elsewhere by the authors [22], met with little success due to the vast amount of algebra generated for each term in each matrix. The sheer size of the resulting code (in excess of 100 MB) actually prevented it from compiling, and resort was ultimately made to a full two-dimensional Gauss–Legendre numerical quadrature scheme. This scheme, which was implemented using commercially available software [24], dynamically allocates the number of integration points in a given calculation to ensure that a highly accurate value of the integral is found. This is a particularly useful feature for the current problem where the circumferential arc length $b$ varies as a function of $x$, and constitutes a much greater degree of analytical complexity than is found in similar formulations for cylindrical shells and flat plates. (Although ultimately the same size eigenproblem has to be solved irrespective of whether it is formulated algebraically or numerically, it will come as no surprise to learn that there is a significant run-time penalty to pay—and hence extra CPU cost—when constructing the stiffness and mass matrices *numerically*).

Inter-element compatibility is achieved simply by matching the appropriate generalized co-ordinates (displacement and rotation for the out-of-plane $C_1$ continuity, but only displacement for the in-plane $C_0$ continuity) at common element nodes and along common edges. This procedure ensures the elements are fully conforming and, moreover, facilitates assembly of the global stiffness and mass matrices $\mathbf{K}^{G}$ and $\mathbf{M}^{G}$. (It should be noted that an assembly of elements in the $x$-wise direction will require the appropriate "small end" radii to be specified in successive elements.)

A variety of different boundary conditions may be applied to the panel by nullifying the appropriate generalized co-ordinates from $\mathbf{K}^{G}$ and $\mathbf{M}^{G}$ which correspond to fixed degrees of freedom. Hence any combination of shear diaphragm (D), simple support (S), clamped (C) or free edges (F), or corner point supports (P), can be accommodated in the analysis. Note: in the current formulation, a shear diaphragm permits an in-plane translation across the support, but prevents $w$-wise motion normal to it; a simple support permits rotation of the plate normal about the supporting edge, but prevents all three ($u$, $v$ and $w$) translational freedoms.

By assuming simple harmonic motion and the absence of any external forcing agency, the governing equations of motion for free vibration can be obtained by combining the expressions for the strain and kinetic energy of the panel into a total potential energy expression, and then employing Lagrange's equation. This yields a standard matrix-eigenvalue problem of the form

$$[\mathbf{K}^{G} - \omega^{2}\mathbf{M}^{G}]\{\mathbf{q}\} = \mathbf{0}. \tag{11}$$

The eigensolutions of equation (11) yield the natural frequencies in radian units, rendered here in the most appropriate form for ready comparison with the work of others and with the experimental results. Corresponding to each eigenvalue is an eigenvector which may be used in conjunction with equation (5) to recover the associated displacement field of each element in the model, and hence the complete mode of the panel under consideration.

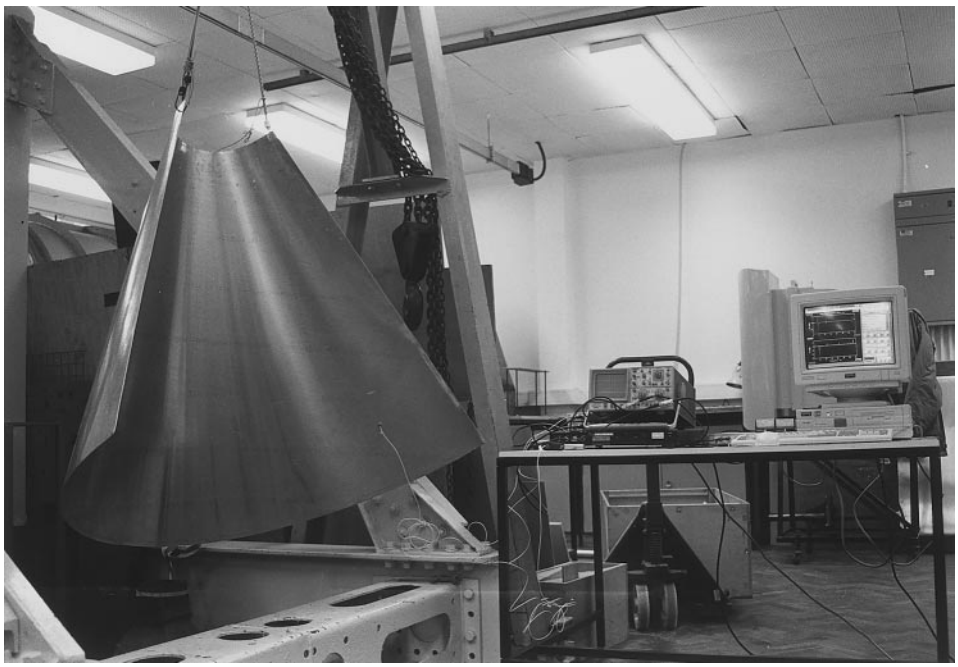

Figure 2. Photograph showing the experimental testing of a freely suspended conical panel.

## 3. INITIAL RESULTS: CONVERGENCE STUDIES FOR F–F–F–F PANELS AND VALIDATION FROM EXPERIMENTAL TESTS

In view of the limited work that has been carried out in this general subject area, it was decided that some experimental work would provide a valuable reference datum for the subsequent theoretical study (see Figures 2 and 3). Completely free edge conditions were selected for this exercise because (i) it is the easiest configuration to test in a laboratory environment, and (ii) it is the most exacting proof of any proposed theoretical solution scheme. To this end, two different aluminium conical panels were produced for testing, which will henceforth be referred to as Cone # 1 and Cone # 2; their geometric and material properties are summarized in Table 2.

For the theoretical analysis, it was first considered germane to undertake a convergence study using three different $h$ meshes, each with different amounts of $p$-enrichment, for the shallow Cone # 1. The frequencies of the first ten elastic modes are presented in Table 3. As would be expected, the frequency parameters are seen to converge monotonically from above, yielding upper bounds to the exact values. The various mixtures of the $h$- and $p$-parameters were chosen to reveal the effect of systematically refining the $h$-mesh at the expense of $p$-enrichment. The term $MO$ refers to the final order of the matrix-eigenvalue problem solved. Such a strategy clearly reveals the greater efficiency of the single super-element, which concurs with other observations [15]. (A fully converged set of frequencies generated from a $20 \times 20$ mesh of SHELL 63 elements in ANSYS 5.3 [25] is included in the final column of Table 4 for additional comparison purposes.) Obviously, in any given study, the number of elements, and degree of

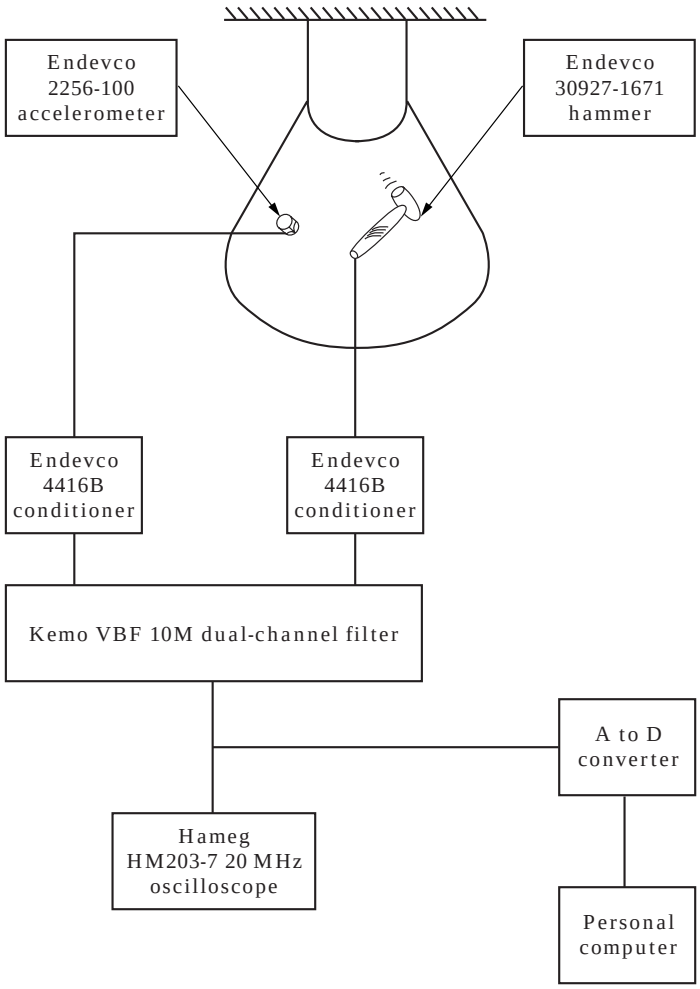


Figure 3. Schematic showing the data acquisition equipment used to capture the test data from the experiment shown in Figure 2.

*p*-enrichment, required to obtain a converged solution will be *highly dependent* on the cone *geometry*. However, for Cone # 2, converged solutions arising from a variety of mesh designs revealed that the most economical solution was still forthcoming from a single super-element boosted to $p = 16$. In general, however, different mesh combinations should always be considered.

The first ten theoretically calculated elastic modes of both conical panels are shown in Figure 4. Referring to the shallow Cone # 1, it might initially be

TABLE 2

*The physical properties of the two conical panels used for experimental purposes*

| | $\alpha$ (deg) | $a$ (m) | $R_0$ (m) | $\phi$ (deg) | $h$ (mm) | $E$ (N/m$^2$) | $\rho$ (kg/m$^3$) | $v$ |
|---|---|---|---|---|---|---|---|---|
| Cone #1 | 3·8 | 1·14 | 0·34 | 130 | 2·0 | 70E9 | 2700 | 0·3 |
| Cone #2 | 26·5 | 1·12 | 0·16 | 180 | 2·0 | 70E9 | 2700 | 0·3 |

TABLE 3

*Convergence study based on three different mesh designs. The first ten elastic frequencies of F–F–F–F Cone # 1*

| | 1 | | 4 | | 9 | | |
|---|---|---|---|---|---|---|---|
| $h$ | | | | | | | 400 |
| $p$ | 8 | 16 | 3 | 6 | 2 | 4 | 0 |
| $f_1$ (Hz) | 7·25 | 7·21 | 7·27 | 7·22 | 7·24 | 7·21 | 7·22 |
| $f_2$ (Hz) | 12·70 | 12·32 | 12·80 | 12·36 | 12·53 | 12·34 | 12·30 |
| $f_3$ (Hz) | 18·59 | 18·21 | 18·73 | 18·25 | 18·45 | 18·23 | 18·21 |
| $f_4$ (Hz) | 34·49 | 34·40 | 35·94 | 34·67 | 35·59 | 34·64 | 34·42 |
| $f_5$ (Hz) | 44·48 | 44·32 | 46·12 | 44·60 | 45·66 | 44·57 | 44·35 |
| $f_6$ (Hz) | 68·22 | 67·78 | 72·57 | 68·46 | 69·93 | 68·22 | 67·78 |
| $f_7$ (Hz) | 76·41 | 75·43 | 77·34 | 75·70 | 76·65 | 75·61 | 75·30 |
| $f_8$ (Hz) | 76·61 | 76·05 | 78·09 | 76·22 | 77·00 | 76·18 | 75·98 |
| $f_9$ (Hz) | 88·32 | 87·80 | 93·80 | 88·51 | 90·18 | 88·27 | 87·76 |
| $f_{10}$ (Hz) | 114·13 | 113·65 | 115·70 | 113·97 | 118·62 | 114·58 | 113·53 |
| *MO* | 432 | 1200 | 456 | 1008 | 644 | 1280 | 2646 |

supposed that the modal behaviour of this particular panel will be very similar to that of an equivalent cylindrical panel. However, it is evident from the modes presented in Figure 4(a) that even a modest amount of conicity markedly alters the behaviour of what might mistakenly have been described as a nominally cylindrical panel—modes 6, 9, and 10 clearly reveal how the opposite curved ends can vibrate with a different number of half waves in the circumferential direction, a feature that is never observed on a genuine cylindrical shell. This effect becomes more pronounced as the semi-vertex angle $\alpha$ is increased, as evidenced by modes 6–10 of Cone # 2 shown in Figure 4(b).

TABLE 4

*The first ten elastic frequencies of both F–F–F–F conical panels*

| | *h-p* | | ANSYS | | Experiment | |
|---|---|---|---|---|---|---|
| | Cone #1 | Cone #2 | Cone #1 | Cone #2 | Cone #1 | Cone #2 |
| $f_1$ (Hz) | 7·21 | 4·65 | 7·22 | 4·31 | 7·5 | 4·5 |
| $f_2$ (Hz) | 12·32 | 8·75 | 12·30 | 8·58 | 12·7 | 8·9 |
| $f_3$ (Hz) | 18·21 | 11·32 | 18·21 | 11·28 | 18·2 | 11·5 |
| $f_4$ (Hz) | 34·40 | 20·85 | 34·44 | 20·63 | 35·6 | 20·9 |
| $f_5$ (Hz) | 44·32 | 22·63 | 44·36 | 21·92 | 46·0 | 21·7 |
| $f_6$ (Hz) | 67·78 | 33·06 | 67·81 | 32·71 | 59·5 | 33·2 |
| $f_7$ (Hz) | 75·43 | 47·83 | 75·31 | 46·68 | 70·4 | 46·6 |
| $f_8$ (Hz) | 76·05 | 47·87 | 75·98 | 47·20 | 73·1 | 47·4 |
| $f_9$ (Hz) | 87·80 | 63·51 | 87·76 | 63·16 | 90·4 | 58·6 |
| $f_{10}$ (Hz) | 113·65 | 67·95 | 113·57 | 66·46 | N/A | 63·7 |

For Cones #1 and 2: $h = 1$ and $p = 16$ giving a total $MO = 1200$.

For the experimental work, a comprehensive series of simple tap tests was performed on both conical shells. Each shell was suspended vertically, with the narrow end uppermost, using one (or two) soft elastic cords suspended from a rigid A-frame to permit both symmetric and asymmetric suspension possibilities. See Figures 2 and 3 for a full description of the rig arrangement and the measurement system used for data acquisition. A broad-band excitation was delivered by tapping the shell with an instrumented hammer, and the response monitored by a wax-mounted lightweight accelerometer. A number of different tapping and monitoring positions was used to capture the modal response. A short time-history of the input and response signals was acquired and subsequently used as the basis for a FFT analysis; this was carried out using a signal processing routine within the MATLAB environment. Natural frequencies were identified from the resonant peak and phase-shift information available from the resulting frequency–response function. Typical results are presented in Table 4, alongside the theoretically derived data. No attempts were made experimentally to determine the modes of vibration.

Very good agreement is found between the results arising from the current work, experimental data, and a proprietary FE package, with the largest discrepancies of 14% arising in the comparison between the theoretical and experimental results for the 6th mode of Cone #1, and 10% arising in the comparisons between the theoretical and experimental results for the 9th mode of Cone #2. The discrepancies may be attributed to the fact that neither experimental sample was perfectly conical, and that the stiffness of the suspension bungies may have exerted some influence on the notionally free edge conditions. However, the level of agreement shown in Table 4 instils confidence in the solution scheme advanced here, and confirms its suitability for use in further parameter studies.

## 4. FURTHER RESULTS AND PARAMETER STUDIES

### 4.1. COMPARISON WITH OTHER WORK

As mentioned in Section 1, only two† pertinent references are currently available which specifically address the subject of free vibration of thin, isotropic, conical panels. These papers, written by Cheung *et al*. [14], and Lim and Liew [15], and the results presented therein, form the basis of a comparison study intended to furnish further confidence with the *h-p* methodology.

The first comparison study concerns the work of Cheung *et al*. [14], who analysed the clamped conical panel (which was originally specified by Srinivasan and Krishnan [13]) defined in the current nomenclature by $a/s = 0{\cdot}6$, $a/h = 100$, $a/R_0 = 3$, $\alpha = 30^\circ$, $\phi = 60^\circ$, and $\nu = 0{\cdot}3$. They presented non-dimensional frequency results according to $\Omega = \omega a^2(\rho h/D)^{1/2}$, and demonstrated monotonic convergence across the first four modes as both the number of finite strips, and the number of sections into which each finite strip is divided, was increased. The most highly converged frequencies arising from Cheung *et al*.'s work are presented in Table 5, alongside those from the current *h-p* methodology, which were

†The work of Srinivasan and Krishnan [13] has not been included here for the reasons mentioned in Section 1, namely, the absence of reliably converged results.

(a)

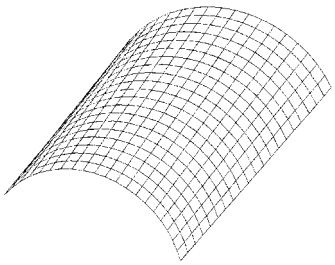

Mode 1: $f$=7.21 Hz

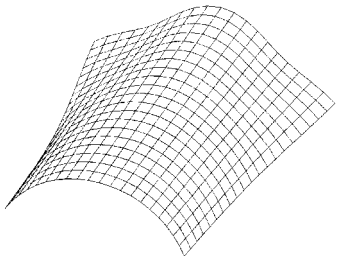

Mode 6: $f$=67.78 Hz

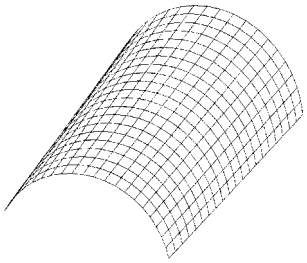

Mode 2: $f$=12.32 Hz

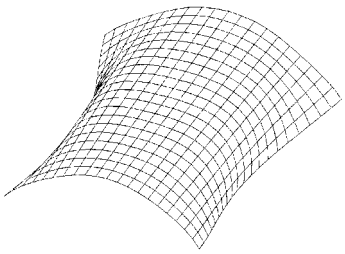

Mode 7: $f$=75.43 Hz

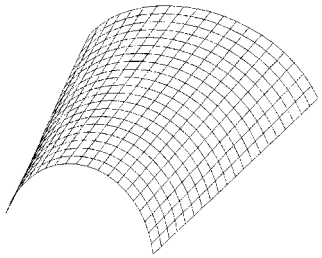

Mode 3: $f$=18.21 Hz

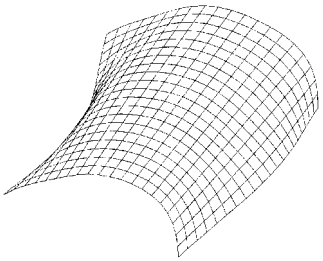

Mode 8: $f$=76.05 Hz

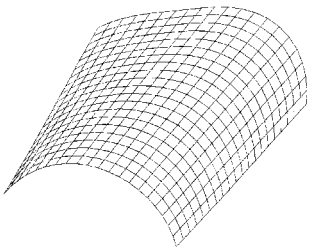

Mode 4: $f$=34.40 Hz

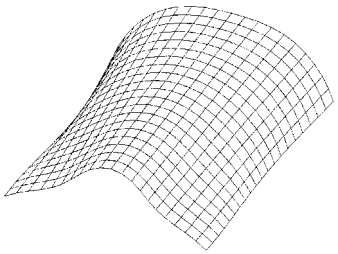

Mode 9: $f$=87.80 Hz

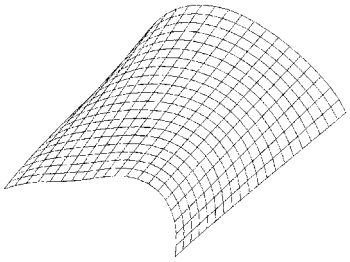

Mode 5: $f$=44.32 Hz

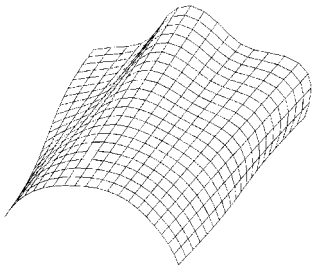

Mode 10: $f$=113.65 Hz

Figure 4(a). *Caption on opposite page*

(b)

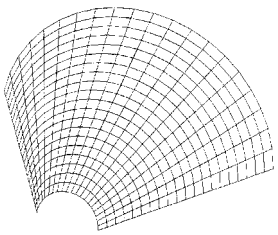

Mode 1: $f$=4.65 Hz

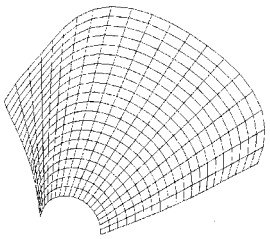

Mode 6: $f$=33.06 Hz

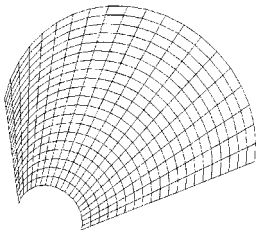

Mode 2: $f$=8.75 Hz

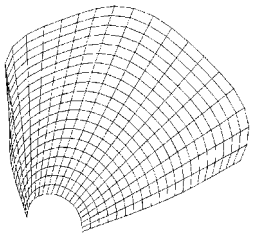

Mode 7: $f$=47.83 Hz

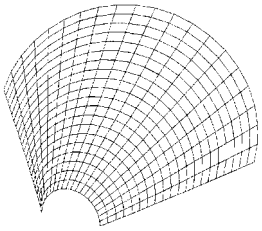

Mode 3: $f$=11.32 Hz

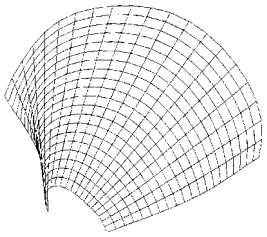

Mode 8: $f$=47.87 Hz

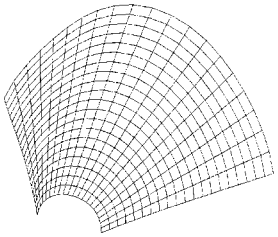

Mode 4: $f$=20.85 Hz

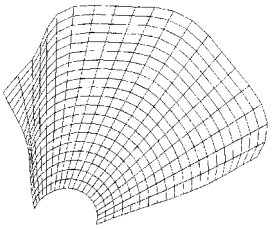

Mode 9: $f$=64.51 Hz

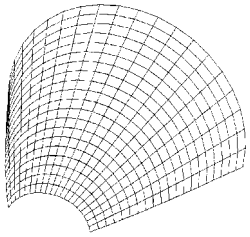

Mode 5: $f$=22.63 Hz

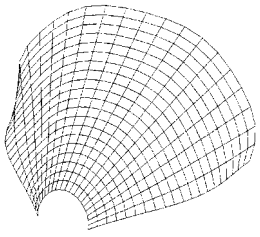

Mode 10: $f$=70.95 Hz

Figure 4(b).

Figure 4. (a) Theoretically computed modes for Cone # 1. (b) The theoretically computed modes for Cone # 2.

TABLE 5

*The first four non-dimensional frequency parameters* $\Omega = \omega a^2(\rho h/D)^{1/2}$ *for a clamped conical shell defined as* $a/s = 0{\cdot}6$, $a/h = 100$, $a/R_0 = 3$, $\alpha = 30^\circ$, $\phi = 60^\circ$, *and* $\nu = 0{\cdot}3$. *Comparison of the h-p results with those generated by Cheung et al.* [14]

| | $\Omega_1$ | $\Omega_2$ | $\Omega_3$ | $\Omega_4$ |
|---|---|---|---|---|
| *h-p* ($h = 1$, $p = 10$) | 210·58 | 260·08 | 309·33 | 355·56 |
| *h-p* ($h = 1$, $p = 16$) | 209·84 | 257·11 | 307·90 | 351·90 |
| Cheung *et al.* [14] | 213·4 | 262·5 | 314·7 | 358·6 |

calculated using a single super element hierarchically enriched firstly with $p = 10$, and secondly with $p = 16$, for all three displacement fields in both the $\xi$- and $\eta$-directions. Excellent agreement is obtained, with the results from the current work being marginally lower than those of Cheung *et al.*; maximum difference of just 2% is observed. This level of agreement, obtained for a conical panel with a moderate semi-vertex angle, helps corroborate the validity of the *h-p* methodology advanced here.

The second comparison study concerns the work of Lim and Liew [15], who deliberately restricted their analysis to *shallow* cones with *trapezoidal* planforms; the formulation they adopted requires a little manipulation to ensure a genuine like-for-like comparison with the present work. (The nomenclature adopted byLim and Liew will be retained in this section only, and explained where necessary.)

Four example cases are considered here, all with a cone semi-vertex angle, $\alpha$, of $7{\cdot}5^\circ$:

(i) CFFF, $\theta_0 = 30^\circ$, $a/s = 0{\cdot}2$;
(ii) CFFF, $\theta_0 = 30^\circ$, $a/s = 0{\cdot}8$;
(iii) CCCC, $\theta_0 = 20^\circ$, $a/s = 0{\cdot}2$;
(iv) CCCC, $\theta_0 = 20^\circ$, $a/s = 0{\cdot}8$;

(The CFFF cases had the larger radius end clamped.) The parameter $\theta_0$ is the base subtended angle of Lim and Liew's formulation, which is related (see [15]) to the base subtended angle $\phi$ in this work by the relationship $\cos\alpha = \tan(\theta_0/2)/\tan(\phi/2)$. Hence, to obtain a strict comparison, the base subtended angles used in the current work were calculated to be $\phi = 30{\cdot}247^\circ$ for cases (i) and (ii), and $\phi = 20{\cdot}169^\circ$ for cases (iii) and (iv).

Results for the frequency parameter $\lambda = \omega a b_0(\rho h/D)^{1/2}$ are presented for the first eight modes of each case in Table 6. (Lim and Liew's parameter $b_0$ is the *projected* length of the base subtended arc length on the trapezoidal planform of the shallow cone.) On closer inspection, it is apparent that the results from the *h-p* methodology are consistently lower than Lim and Liew's results, especially the fundamental and first few overtone frequencies†, whilst broad general agreement

†For example, the fundamental frequency of case (ii) cantilevered panel as calculataed by the *h-p* methodology is 0.53 times that calculated by Lim and Liew. The corresponding mode is shown in Figure 5(a); with such an extreme aspect ratio, it is not surprising that this mode is slow to converge.

is found at the higher frequencies. Such a discrepancy was a cause for concern, especially since there are no other comparable results in the literature against which further checks could be made. Hence, to obtain independent arbitration, it was decided to construct a detailed finite element model using the 4-noded SHELL-63 elements available in ANSYS [25], and to include these additional results for completeness (see Table 6). From this study, the ANSYS results confirm the validity of the results arising from the *h-p* methodology, and suggest a lack of convergence in Lim and Liew's work. Upon further reflection, this would seem the most likely explanation, especially in view of the extreme aspect ratios considered by Lim and Liew. For example, the CCCC case (iv) is such that an ANSYS mesh of 350 elements along the length and 25 elements around the circumference was necessary to obtain a converged set of results from ANSYS whilst ensuring the individual element aspect ratios were not excessively distorted! The results for this particular case are most illuminating: e.g., the fundamental mode consists of a small "bulge" extending no more than 10% of the panel length and localized at the base end of the panel [see Figure 5(b)]. This adds weight to the conjecture that Lim and Liew's results are not fully converged, since their methodology is based upon the use of *global* functions, and would therefore require the use of extremely short wavelength assumed displacement functions to "capture" such a localized mode; there is no evidence they used such high order modes. In the light of this, the usefulness of Lim and Liew's results as benchmark data must be questioned.

This exercise highlights two important problems associated with the dynamic behaviour of conical shells: (i) if extreme geometries are considered, highly localized modes of vibration are likely to result, and these will prove difficult to model accurately without *a priori* knowledge; and (ii) the *h*-mesh/*p*-boost design which gives fully converged frequencies for one particular cone geometry almost certainly will not give similarly converged frequencies for a different geometry, so in general it will be necessary to validate the convergence of each and every case.

### 4.2. RESULTS FROM AN INITIAL PARAMETER STUDY

In view of the large number of parameter combinations that could be studied, it was decided to limit the scope of the current work to an investigation of just one variable, namely the effect on frequency of varying the cone semi-vertex angle $\alpha$. This variable was chosen simply because it demonstrates most clearly the effects of "conicity" in a given panel. Two different sets of boundary conditions were considered for the panel under consideration, namely (i) simply supported around all four edges, and (ii) fully clamped around all four edges, since such combinations probably yield respectively the extremes of flexibility and stiffness that could be realized in practice by the frames and stringers of a typical sub-structure. The physical dimensions attributed to the following [fixed] panel parameters are representative of those found in civil aviation structural specifications: $a/h = 333{\cdot}33$, $a/R_0 = 2$, $\phi = 60^\circ$, $E = 70$ GPa, $\rho = 2800$ kg/m$^3$, and $\nu = 0{\cdot}3$. (It should be noted that when $\alpha = 0^\circ$, a cylindrical shell of mass $2\pi\rho h R_0^2/3$ results; when $0^\circ < \alpha < 90^\circ$, a generic conical panel results, with an increasing radius at the large end and hence an increasing surface area—the mass of this

TABLE 6

*The frequency parameter* $\lambda = \omega a b_0 (\rho h/D)^{1/2}$ *for various shallow conical shells with* $\nu = 0{\cdot}3$, $s/h = 1000$, *and* $\alpha = 7{\cdot}5^\circ$. *A comparison of the h-p results with those generated by a proprietary finite element package, and Lim and Liew* [15]

| B/C | $\theta_0$ | $\phi$ | $a/s$ | Method | $\lambda_1$ | $\lambda_2$ | $\lambda_3$ | $\lambda_4$ | $\lambda_5$ | $\lambda_6$ | $\lambda_7$ | $\lambda_8$ |
|---|---|---|---|---|---|---|---|---|---|---|---|---|
| CFFF | 30° | 30·247° | 0·2 | *h-p* | 5·5130 | 8·9563 | 26·989 | 28·852 | 50·174 | 64·497 | 75·479 | 79·578 |
| | | | | ANSYS | 5·5179 | 8·9608 | 27·014 | 28·909 | 50·267 | 64·631 | 75·541 | 79·815 |
| | | | | [15] | 6·1727 | 9·0708 | 27·299 | 29·758 | 50·669 | 65·171 | 74·499 | 80·201 |
| CFFF | 30° | 30·247° | 0·8 | *h-p* | 1·6855 | 6·3789 | 15·158 | 16·412 | 23·937 | 28·076 | 38·344 | 45·069 |
| | | | | ANSYS | 1·6841 | 6·3881 | 15·201 | 16·363 | 23·928 | 28·191 | 38·232 | 45·324 |
| | | | | [15] | 3·2691 | 8·3659 | 16·521 | 17·117 | 23·907 | 29·891 | 38·614 | 46·687 |
| CCCC | 20° | 20·169° | 0·2 | *h-p* | 235·35 | 247·45 | 258·64 | 269·32 | 280·39 | 294·21 | 302·82 | 312·74 |
| | | | | ANSYS | 234·90 | 246·74 | 257·71 | 268·17 | 278·85 | 291·94 | 301·67 | 309·57 |
| | | | | [15] | 239·10 | 251·32 | 262·61 | 273·37 | 284·46 | 298·19 | 306·17 | 316·56 |
| CCCC | 20° | 20·169° | 0·8 | *h-p* | 941·79 | 990·29 | 1035·1 | 1077·8 | 1119·3 | 1160·3 | 1200·9 | 1212·9 |
| | | | | ANSYS | 940·34 | 988·07 | 1032·3 | 1074·4 | 1115·5 | 1155·9 | 1196·1 | 1206·4 |
| | | | | [15] | 956·57 | 1006·0 | 1055·8 | 1120·3 | 1206·1 | 1225·0 | 1284·8 | 1337·6 |

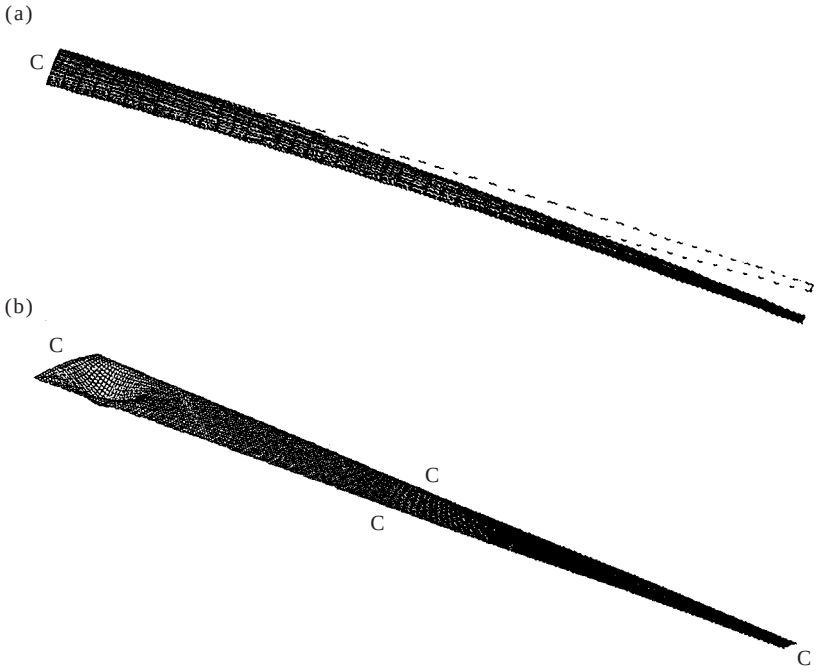


Figure 5. (a) Fundamental mode of a CFFF extreme geometry conical panel, after [15]. (b) Fundamental mode of a CCCC extreme geometry conical panel, after [15].

generic panel is $2\pi\rho hR_0^2(1 + \sin\alpha)/3$; and when $\alpha = 90^\circ$, a flat sectorial plate of mass $4\pi\rho hR_0^2/3$ results.)

The mesh design chosen for this particular problem consisted of dividing the panel circumferentially into three equal lengthwise elements, each $p$-enriched with a total of 10 hierarchical functions applied in each co-ordinate direction (see the illustration accompanying Table 7). The rationale behind this design was in recognition of the fact that most modes of the curved panels would primarily involve deformations around the circumference, so by sub-dividing the panel accordingly, it would be possible to capture such motion relatively easily and at minimal expense. This reasoning is confirmed in Table 7, where the results from the current $h$-$p$ methodology for the extreme cases of a cylindrical shell and a sector plate correlate surprisingly well with those from an ANSYS analysis, yet at a fraction of the computational effort.

Frequency trends for the first six modes, rendered in terms of the non-dimensional frequency $\Omega = \omega a^2(\rho h/D)^{1/2}$ versus cone semi-vertex angle $\alpha$, are presented in Figure 6 for the simply supported panel, and in Figure 7 for the clamped panel.

Both figures show remarkably similar trends for the frequencies of the first six modes of vibration of each panel, with the frequencies from the clamped case being only marginally higher than the corresponding ones from the simply supported case. At first sight, this seemed a little unusual, and further verification was sought by using ANSYS to determine the frequencies for the two limiting cases encountered here of a cylindrical shell and a sectorial plate. The results for these

TABLE 7

*A comparison and verification of the "limiting case" frequencies from the results shown in Figures 6 and 7*

| Limiting case | Method | S–S–S–S | | | | | | C–C–C–C | | | | | |
|---|---|---|---|---|---|---|---|---|---|---|---|---|---|
| | | $\Omega_1$ | $\Omega_2$ | $\Omega_3$ | $\Omega_4$ | $\Omega_5$ | $\Omega_6$ | $\Omega_1$ | $\Omega_2$ | $\Omega_3$ | $\Omega_4$ | $\Omega_5$ | $\Omega_6$ |
| $\alpha = 0^\circ$ (Cylindrical shell) | *h-p* FEM | 388·1 | 479·0 | 588·8 | 626·2 | 674·9 | 778·3 | 456·2 | 487·0 | 622·3 | 689·5 | 794·3 | 838·5 |
| | ANSYS | 387·6 | 478·9 | 587·7 | 625·2 | 672·2 | 775·6 | 455·7 | 484·7 | 617·6 | 685·6 | 790·2 | 828·5 |
| $\alpha = 90^\circ$ (Sectorial plate) | *h-p* FEM | 19·2 | 43·6 | 50·9 | 78·9 | 83·3 | 101·1 | 35·2 | 66·3 | 74·9 | 108·4 | 113·2 | 134·9 |
| | ANSYS | 19·1 | 43·5 | 50·7 | 78·6 | 82·9 | 100·6 | 35·0 | 66·0 | 74·4 | 107·7 | 112·2 | 133·0 |

**Mesh data for *h-p* FEM results:**

$p = 10$ per element in each co-ordinate direction, $h = 3$, as indicated. (Dashed line denotes lengthwise element boundaries.) This mesh gives rise to final matrix orders of 592 (S-S-S-S) and 532 (C-C-C-C) for both the sector plate and the cylindrical shell.

**Mesh data for *ANSYS* FEM results:**

Cylindrical shell: $h = 900$ ($30 \times 30$) using 4-noded SHELL-63 elements. This mesh gives rise to final matrix orders of 5406 (S-S-S-S) and 5046 (C-C-C-C).

Sector plate: $h = 400$ ($20 \times 20$) using 4-noded SHELL-63 elements. This mesh gives rise to final matrix orders of 2160 (S-S-S-S) and 1920 (C-C-C-C).

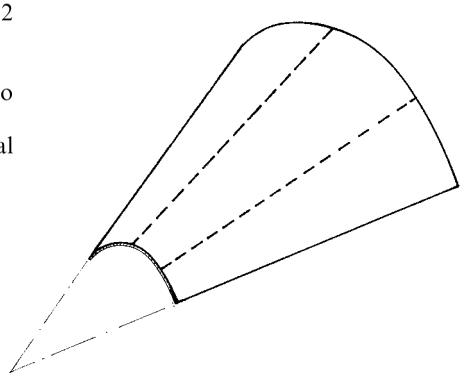

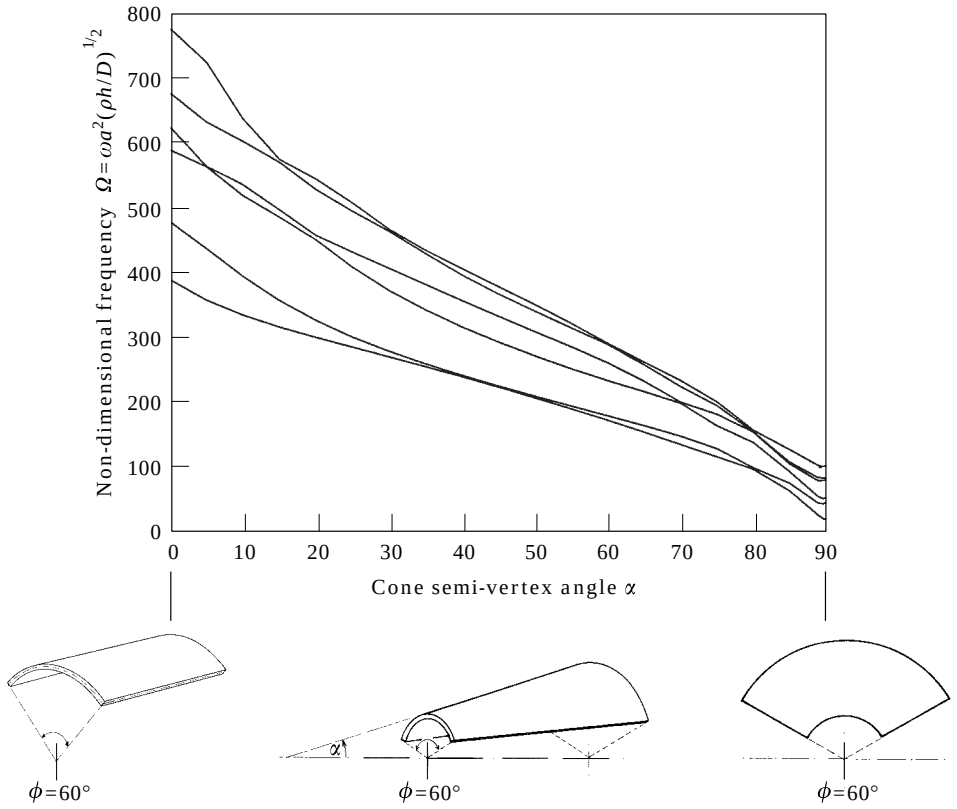


Figure 6. Frequency trends for the first six modes of a conical panel, showing non-dimensional frequency $\Omega$ versus cone semi-vertex angle $\alpha$. All edges S–S–S–S.

cases are presented in Table 7, where very good agreement can clearly be seen. Such a comparison is most helpful in confirming the validity of the results presented in Figures 6 and 7, especially in the light of the unusual dynamic behaviour associated with these conical panels.

From Figures 6 and 7, it is evident that the frequencies of a given mode reduce with increasing $\alpha$, and there are two principal reasons for this: (i) as the larger end radius is increased, the panel's effective bending stiffness decreases for modes which are aligned along a generator (modes aligned around the circumference will not greatly be affected by this effect for the reasons described in detail in [22]); and (ii) the mass of the panel is *doubled* as $\alpha$ is varied from $0^\circ$ to $90^\circ$, this increase occurring as a sinusoidal function of semi-vertex angle, $\alpha$. It is this combined effect of increasing mass (which is almost certainly the dominant factor here) and decreasing flexural rigidity along the generator that is responsible for the natural frequencies reducing with increasing semi-vertex angle $\alpha$.

## 5. CONCLUSIONS

An initial study of the vibration characteristics of open, conically curved, isotropic shell panels has been undertaken using the *h-p* version of the finite

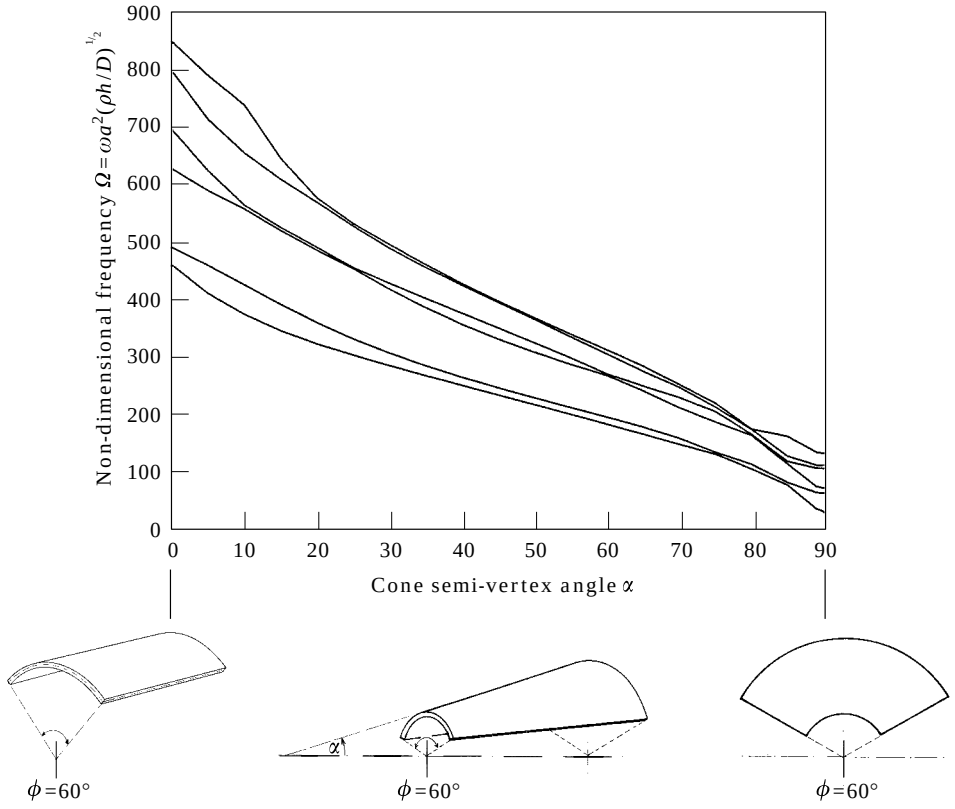


Figure 7. Frequency trends for the first six modes of a conical panel, showing non-dimensional frequency $\Omega$ versus cone semi-vertex angle $\alpha$. All edges C–C–C–C.

element method. The convergence properties of this shell element have been established for particular geometries, thereby endorsing its suitability for use in further parameter studies. Natural frequencies and modes have been obtained for two completely free panels using (i) the *h-p* methodology reported here, (ii) a commercially available finite element package, and (iii) experimental work. Excellent agreement has been found between all three approaches. Some further comparisons with the work of other investigators have also been performed, and generally good agreement has been found. Where differences have been identified, further verification has been sought using the finite element package ANSYS , and the source of the problem has been traced to insufficiently converged results in the work of other investigators. Finally, a brief parameter study has been presented for clamped and simply supported conical panels, whose semi-vertex angle $\alpha$ has been varied between $0^\circ$ and $90^\circ$.

This work has highlighted some interesting nuances associated with the dynamic behaviour of conical shells. Firstly, if extreme geometries are considered, highly localized modes of vibration are likely to result, and these will prove difficult to model accurately without *a priori* knowledge. Secondly, the level of mesh refinement which gives fully converged frequencies for one particular cone

geometry almost certainly will not give similarly converged frequencies for a different geometry, so in general it will be necessary to validate the convergence of each and every case. This is especially important for conical panels, since their vibration behaviour is quite different from cylindrical panels, and it does not seem possible to predict what effect a certain parameter change will have on a conical panel, even if its effect on a similar cylindrical panel is known.

Regarding the current *h-p* finite element formulation derived in this paper, it has been observed that its overall performance exceeds that of a more general commercial software package. Perhaps this is not surprising when it is understood that the work presented here is tailored specifically to conical panels, whereas the commercial package makes use of a more general shell element. Even so, it is worth noting that by using the *h-p* version of the FEM in preference to the *h*-version, it is possible to obtain converged answers using some 50% fewer degrees of freedom (see Table 3). Finally, it is worth pointing out that the methodology advanced here for a generic conical panel can also be used to analyse closed conical frusta, open or closed cylindrical shells ($\alpha = 0^\circ$, $R_0 = R_A$ set to the radius of the cylinder), flat annular sectorial plates ($\alpha = 90^\circ$, $R_0$ set to the inner radius and $R_A$ set to the outer radius of the plate), and flat sectorial wedge plates ($\alpha = 90^\circ$, $R_0$ set to an extremely small value ($\approx 0$) and $R_A$ set to the radius of the plate).

## ACKNOWLEDGMENTS

The assistance rendered by the following companies and individuals is gratefully acknowledged: EPSRC, under contract number GR/J 06306, for providing the financial support; the Composites Workshop of British Airways Engineering, Heathrow Airport, for producing the test specimens; and Messrs J. R. Smith and G. S. Aglietti, of the Department of Aeronautics and Astronautics, for producing the ANSYS results.

## REFERENCES

1. C. H. Chang 1981 *The Shock and Vibration Digest* **13**, 9–17. Vibrations of conical shells.
2. A. W. Leissa 1973 *Vibration of Shells*. NASA SP288 (Chapter 5).
3. A. E. H. Love 1927 *A Treatise on the Mathematical Theory of Elasticity*. New York: Dover, fourth edition.
4. M. J. O. Strutt 1933 *Annalen der Physik* **17**, 729–735. Free vibration of conical shells.
5. A. T. van Urk and G. B. Hut 1933 *Annalen der Physik* **17**, 915–920. Radial vibrations of aluminium cones.
6. N. W. McLachlan 1934 *Loudspeakers*. Oxford: Clarendon Press.
7. W. C. L. Hu 1964 Technical Report No. 1, Contract NASr-94(06), Southwest Research Institute. A survey of the literature on the vibrations of thin shells.
8. C. T. Tang 1964 *Scientia Sinica* **13**, 1192–1210. The vibration modes and eigenfrequencies of circular conical (and cylindrical) shells.
9. V. I. Weingarten 1965 *ASCE Journal of Engineering*, *Mechanical Division* **91**(EM4), 69–87. Free vibrations of conical shells.
10. K. M. Liew, C. W. Lim and S. Kitipornchai 1997 *Applied Mechanics Review* **50**, 431–444. Vibration of shallow shells: a review with bibliography.

11. J. N. Rossettos and R. F. Parisse 1969 *Transactions of ASME*, *Journal of Applied Mechanics*, Paper No. 69-APM-22. The dynamic response of cylindrical and conical panels.
12. D. Teichmann 1985 *American Institute of Aeronautics and Astronautics Journal* **23**, 1634–1637. An approximation of the lowest eigen frequencies and buckling loads of cylindrical and conical shell panels under initial stress.
13. R. S. Srinivasan and P. A. Krishnan 1987 *Journal of Sound and Vibration* **117**, 153–160. Free vibration of conical shell panels.
14. Y. K. Cheung, W. Y. Li and L. G. Tham 1989 *Journal of Sound and Vibration* **128**, 411–422. Free vibration analysis of singly curved shell by spline finite strip method.
15. C. W. Lim and K. M. Liew 1995 *Engineering Structures* **17**, 63–70. Vibratory behaviour of shallow conical shells by a global Ritz formulation.
16. K. M. Liew, M. K. Lim, C. W. Lim, D. B. Li and Y. R. Zhang 1995 *Journal of Sound and Vibration* **180**, 271–296. Effects of initial twist and thickness variation on the vibration behaviour of shallow conical shells.
17. C. W. Lim and K. M. Liew 1996 *International Journal of Solids and Structures* **33**, 451–468. Vibration of shallow conical shells with shear flexibility: a first-order theory.
18. C. W. Lim, K. M. Liew and S. Kitipornchai 1998 *International Journal of Solids and Structures* **35**, 1695–1707. Vibration of cantilevered laminated composite shallow conical shells.
19. O. C. Zienkiewicz, J. P. De, R. Gago and D. W. Kelly 1983 *Computers and Structures* **16**, 53–65. The hierarchical concept in finite element analysis.
20. I. Babuska and B. Guo 1986 *Computational Mechanics* **1**, 21–41. The *h-p* version of the finite element method, Part 1: the basic approximation results.
21. O. Beslin and J. Nicolas 1997 *Journal of Sound and Vibration* **202**, 633–655. A hierarchical functions set for predicting very high order plate bending modes with any boundary conditions.
22. N. S. Bardell, R. S. Langley and J. M. Dunsdon 1997 *Journal of Sound and Vibration* **207**, 647–669. On the free vibration of completely free, open, cylindrically curved, isotropic shell panels.
23. W. Soedel 1993 *Vibrations of Shells and Plates*. New York: Dekker, second edition.
24. *D*01*AKF*. *The NAG FORTRAN Workshop Library Handbook—Release* 1. Oxford: NAG, 1986.
25. *ANSYS version* 5.3, 201 Johnson Road, Houston, PA 15342-1300, U.S.A.